Original article
https://doi.org/10.18019/1028-4427-2025-31-1-28-41

Possible application of glassy carbon composite scaffolds in bone tissue engineering

E.I. Timoshchuk, D.V. Ponomareva✉, A.R. Gareev

Research Institute of Structural Materials Based on Graphite "NIIgrafit", Moscow, Russian Federation

Corresponding author: Daria V. Ponomareva, DVPonomareva@rosatom.ru

Annotation

Introduction Bone defect management remains one of the challenging problems of regenerative medicine, for the solution of which the most promising trend is the use of tissue-engineered implants based on composite scaffolds that stimulate osteogenesis. One of the main tasks of tissue engineering is the development of a scaffold that mimics three-dimensional architecture for osteogenic progenitor cells inside the scaffold, with the possibility of cell interaction with appropriate chemical and physical stimuli of natural bone.

The **purpose** of the work is to evaluate the possibility of using composite scaffolds based on glassy carbon in tissue engineering.

Materials and methods This study describes a reproducible method of obtaining three-dimensional porous glass-carbon-based scaffolds with surfaces modified with pyrocarbon (CF-C) and pyrocarbon and hydroxyapatite (CF-C-HAP) and investigates the porosity, strength characteristics, cytotoxicity, and osteoinductivity of the composite scaffolds obtained. Osteogenic differentiation of cultured human mesenchymal stem cells (MSCs) was evaluated on CF-C and CF-C-HAP scaffolds using common osteogenic markers such as: alkaline phosphatase (ALP) activity, alizarin red staining and quantitative real-time PCR (qPCR).

Results *In vitro* studies showed the biocompatibility of the developed scaffolds. The ability of CF-C-HAP to induce MSC differentiation in osteogenic direction and to produce calcium-containing matrix was established.

Discussion The scaffolds based on glassy carbon foam with pyrocarbon and hydroxyapatite coatings have a three-dimensional structure with open porosity, along with the strength comparable to the strength of the replaced tissue, and imitate the structure of trabecular bone. However, the strength of glassy carbon foam without coating is characterized by low compressive strength. All the studied materials demonstrated adhesive and proliferative activity of MSCs, high cell adhesion and absence of cytotoxicity. Determination of the mRNA expression level by real-time PCR showed that after 14 days, cells cultured on CS-C-HAP showed expression of the VDR, BMP7, IGFR1, SPP1 genes, what demonstrates osteogenic potential. The results of our studies on phosphatase activity and alizarin red staining demonstrated that the CF-C-HAP scaffold stimulates osteoblast differentiation *in vitro* in the osteogenic direction, as well as intracellular mineralization processes.

Conclusion Composite CF-C-HAP scaffolds based on glassy carbon foam support cell proliferation and differentiation and may be promising for use in bone tissue engineering.

Keywords: scaffold, glassy carbon, hydroxyapatite, osteogenesis, mesenchymal stromal cells, bone tissue engineering

For citation: Timoshchuk EI, Ponomareva DV, Gareev AR. Possible application of glassy carbon composite scaffolds in bone tissue engineering. *Genij Ortopedii*. 2025;31(1):28-41. doi: 10.18019/1028-4427-2025-31-1-28-41.

INTRODUCTION

Bone is a hard vascularized human organ that performs protective and mechanical support functions. Moreover, bone tissue can be attributed to as a part of the endocrine system: osteocalcin is secreted mainly by osteoblasts and in a decarboxylated form is able to bind to its own receptor on pancreatic beta cells and Leydig cells [1]; FGF23 (fibroblast growth factor 23) is synthesized by osteocytes and is the main regulator of phosphorus-calcium metabolism [1]. Bone tissue has good regenerative properties and is able to restore its structure without fibrous scar tissue. However, in the case of crush injury or aggravating factors, such as old age and/or concomitant somatic diseases, a deviation of bone tissue regeneration from organotypic towards substitution (formation of fibrous and cartilaginous tissue) is possible [2]. In critical size bone defects, independent recovery becomes impossible and surgical intervention is required. Extensive bone tissue defects can be caused by various factors: trauma, tumor and infectious processes, surgical interventions (resection of pathological areas). Besides, the increase in the geriatric population also contributes to the growth of the number of musculoskeletal system diseases.

Traditional approaches to the treatment of critical-size defects include the use of auto- and allografts [3, 4]. Autografts are considered the "gold standard" due to their good osteoinductivity, osteoconductivity, and osseointegration, which promote tissue formation at the defect site [5, 6]. However, the use of autografts has a number of significant disadvantages, such as an increase in the volume of surgical intervention, a limited volume of donor tissue, and an increased risk of postoperative complications (infection, bleeding, and damage to the neurovascular system of the donor site). The disadvantages of allografts include low osteoinductivity, the risk of transmitting infectious diseases from the recipient to the donor, the possibility of developing a histoincompatibility reaction and chronic inflammation, as well as violation of ethical and religious principles [7–9].

In recent years, tissue engineering has been considered a promising alternative to auto- and allografts in the treatment of bone tissue diseases and injuries [10, 11]. The concept of tissue engineering includes three main units: cells, scaffolds, and osteoinductive growth factors [12, 13].

Due to their bioinertness, porous carbon-based materials may be candidates for use as scaffolds. Scaffolds based on hydroxyapatite/porous carbon composite have been reported to promote MG-63 adhesion and proliferation [14]. However, despite this, the use of porous carbon materials as scaffolds is limited due to their low strength properties (the compressive strength of Duacel® carbon foam is 0.47 MPa). Since implantable scaffolds are subjected to various mechanical loads, including compression, tension, torsion, and shear [1], it is extremely important to create a material that is able to withstand the load during the regeneration process.

The **purpose** the work is to evaluate the possibility of using composite scaffolds based on glassy carbon in tissue engineering.

MATERIALS AND METHODS

Composite scaffolds Commercially available phenol-formaldehyde resin powder of the SFP-012A2 brand (Metadinea LLC) was used as a carbon precursor. The phenol-formaldehyde resin powder was dissolved in ethyl alcohol to obtain a solution with a concentration of 30 wt. % for subsequent impregnation of polymer templates (Regicell® PPI 80). The samples were impregnated by immersing them in an alcohol solution of phenol-formaldehyde resin at a temperature of 35–40 °C with treatment in an ultrasonic bath for 30 min, after which the samples were extracted and excess impregnation solution was removed from them by squeezing. The impregnated samples

were dried using forced convection for 15 min at a temperature of 70 °C and then dried in a drying cabinet at temperatures of 70, 90, 120 °C. Curing was carried out at a temperature of 150 °C for 4 hours. Pyrolysis of foam precursors was carried out in a nitrogen atmosphere at a temperature of (1000 ± 50) °C, with a temperature rise rate of 2.5 °C/min and isothermal holding for 30 minutes. As a result of pyrolysis, glassy carbon foam replicating the precursor polymer was obtained. Then the process of pyrolytic carbon deposition on the surface of glassy carbon foam was carried out using the CVI method. Methane (purity 99.9 %, JSC MGPZ, Russia) was used as a precursor gas, the process temperature was (1050 ± 50) °C, the process duration was 20 hours.

Hydroxyapatite coating To grant the material osteoinductive properties, its surface was modified with hydroxyapatite. The operations described below were performed.

A porous carbon scaffold. pyrocarbon coated, with geometric dimensions of 10 × 10 × 20 mm was degreased and cleaned from mechanical impurities by boiling in ethyl alcohol, after which it was washed with distilled water to a neutral pH. The cleaned scaffold was immersed in an electrolyte solution with a component concentration providing a Ca/P ratio of 1.67, the pH was maintained at 3–5, the deposition time was 25 min at a temperature of 40 °C under constant stirring with a magnetic stirrer. A sample of pyrocarbon-coated carbon scaffold, acting as a cathode, was placed in the center of a spiral platinum anode. A Matrix MPS-3020 current source (China) was used for electrochemical deposition. After completion of the electrolytic deposition, the sample was removed and dried in air to constant weight, after which the electrolyte residues were removed by washing in distilled water to neutral pH of the washing water. The washed sample was dried at a temperature of 140 °C to constant weight.

The samples were labeled as follows: CF (carbon foam), C (carbon coating), HAP (hydroxyapatite).

Density and porosity The volumetric density of the samples was calculated as the ratio of mass to volume; the volume was determined by measuring the geometric dimensions of the sample using a digital caliper. Pycnometry using helium was carried out to establish the true density of the carbon "skeleton" on the AccuPyc II 1340 device [13].

Porosity Ƥ (%) and pore volume $V_Ƥ$ (cm^3/g):

$$Ƥ = \left(1 - \frac{\rho_b}{\rho_s}\right) \times 100\ \% \qquad (1)$$

$$V_Ƥ = \frac{1}{\rho_b} - \frac{1}{\rho_s} \qquad (2)$$

where ρ_b — volumetric density; g/cm^3; ρ_s — true density, g/cm^3.

Compressive strength The mechanical properties of the scaffolds were studied at room temperature on a universal testing machine manufactured by Zwick/Roell (Germany) under a constant speed of movement of the active crosshead of 0.5 mm/min.

To conduct the tests to determine the compressive strength, parallelepiped-shaped samples sized 10 × 10 × 20 mm were used.

When preparing (cutting) the samples, treatment of the loading surfaces was assessed. The ends of the samples were made plane-parallel to each other to avoid skewing during loading. Otherwise, destruction could occur at the ends of the sample, and the ultimate strength would be significantly lower than the actual one. To minimize the effect of skewing, the tests were carried out using a special floating support (Fig. 1). During the test, the loading diagram was recorded in the coordinates "Load-Deformation", the ultimate strength σ_{comp} was calculated using the formula:

$$\sigma_{comp}=P_{max}/bh \qquad (3)$$

where: P_{max} — maximum load, H; b — sample width, mm; h — sample thickness, mm.

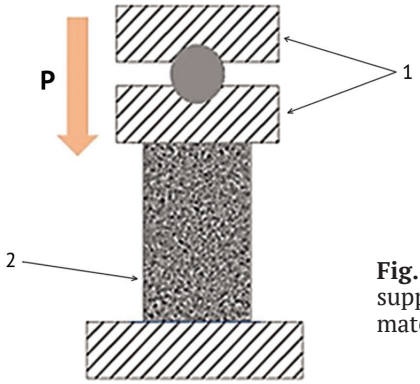

Fig. 1 Loading diagram: 1) floating support; 2) a sample of carbon porous material

To obtain statistically reliable data, the average value of at least five different measurements was obtained and the standard deviation was calculated.

Cell culture The study was performed using a primary culture of human dental pulp mesenchymal stromal cells (DPSCs) which phenotype (CD44+CD54+, CD90+, CD105+, CD34–, CD45–, HLA–DR–, CD31–, CD133–) is consistent with MSCs. The primary culture of human multipotent mesenchymal stromal cells was isolated from the third molar rudiment extracted for orthodontic reasons (DPSCs, Dental Pulp Stem Cells) of a healthy 16-year-old patient. The aseptically extracted tooth rudiment was crushed with scissors to a size of 1–2 mm^3 and dissociated with a solution of 0.25 % trypsin — 0.02 % EDTA (ethylenediaminetetraacetic acid) (PanEco, Russia) for 30 min at 37 °C. The isolated cells were centrifuged for 3 min at 200 g and placed in DMEM/F-12 (Dulbecco's modified Eagles medium, PanEco) culture medium at a 1:1 ratio with the addition of 10 % fetal bovine serum (FBS), transferred to 25 cm^2 flasks and cultured in an atmosphere of 5 % CO_2 at 37 °C in DMEM (PanEco) medium containing 10 % FBS (HyClone), 100 units/ml penicillin/streptomycin and the addition of 2 mM L-glutamine. Upon reaching a subconfluent state, the cells were treated with 0.25 % trypsin-EDTA solution and transferred to 75 cm2 flasks, cultivation was carried out in DMEM / F-12 medium 10 % FBS, 100 units / ml penicillin / streptomycin and the addition of 2 mM L-glutamine in a ratio of 1: 1 (Life technologies, USA) at 37 °C in an atmosphere of 5 % CO_2. As they grew and reached a subconfluent state, the cells were treated with 0.25 % trypsin-EDTA solution and passaged into new flasks in a ratio of 1: 2. Cells at passage 3 were used for the studies.

Citotoxicity The cell viability was studied using the MTT test, which is based on the restoration of a colorless tetrazolium salt (3-[4,5-dimethylthiazol-2-yl]-2,5-diphenyltetrazolium bromide, MTT) by mitochondrial and cytoplasmic dehydrogenases of living metabolically active cells with the formation of blue crystals of formazan, soluble in dimethyl sulfoxide.

After 2 days from the introduction of the extracts of the materials, the culture medium was removed and 100 µl of a 0.5 mg/ml MTT solution in DMEM/F12 culture medium without serum were added to each well. After incubation for 3 hours at 37 °C in a humidified atmosphere of 5 % CO_2, the liquid was removed, 100 µl of dimethyl sulfoxide (DMSO) were added and, shaking the plates at room temperature for 10 min, the formed formazan salts were dissolved. The amount of reduced formazan was determined by the optical density of the solutions on a model 680 photometer (BIO-RAD, USA) at a wavelength of 540 nm. Statistical analysis of the obtained results was performed using the nonparametric Mann – Whitney U-test. The standard deviation from the mean value was taken as an error, differences according to the Mann – Whitney U-test at $p < 0.05$ were taken as reliable.

Viability, adhesive, proliferative and differentiating activity of human MSCs To study the viability, adhesive, proliferative and differentiating activity of human MSCs, the cells were seeded on the surface of the samples at a density of 40 thousand/cm^2 and cultured for 14 days, while the volume of the medium was 0.5 ml/well. The medium was changed every 3–4 days. Differentiating activity of the cells was assessed by determining the degree of calcification and detecting the activity

of alkaline phosphatase in the cells. To determine the viability of the cells, the fluorescent staining method with a mixture of SYTO 9 dyes, propidium iodide and Hoechst 33342 was used. The fluorescent dye SYTO 9 in the study mode λ_{exc} = 450–490 nm, λ_{emiss} = 515–565 nm stained DNA and RNA of living and dead cells in green color. The intercalating reagent propidium iodide in the study mode λ_{exc} = 546 nm, λ_{emiss} = 575–640 nm stained the nuclei of dead cells red. The fluorescent dye Hoechst 33342 in the study mode λ_{exc} = 355 nm, λ_{emiss} = 460 nm stained the DNA of living and dead cells blue. Microphotography of the cells was taken on an Axiovert 200 microscope (Carl Zeiss, Germany).

The degree of calcification was determined by staining calcium phosphate deposits with alizarin red (pH = 4.1). For this purpose, after the end of cultivation, the cells were washed with 0.01 M phosphate buffer (pH = 7.4) and fixed for 20 min. in 3.7 % buffered formaldehyde solution. After removing the fixative and washing with deionized water, the cells were stained with 2 % alizarin red solution for 5 min to detect the formation of mineralized matrix. Cell morphology and the amount of calcifications were assessed using an Axiovert 200 microscope (Carl Zeiss, Germany). Alkaline phosphatase activity was determined using a reagent kit (Alkaline phosphatase kit, Sigma 86-R) according to the manufacturer's instructions. The cells were fixed for 30 sec in citrate-acetone-formaldehyde fixative, washed with deionized water and stained for 15 min with a buffered solution containing naphthol-AS-phosphate, fast red violet (chromogenic substrate used to determine alkaline phosphatase activity). The wells were washed with deionized water and counterstained with hematoxylin solution for 2 min. After washing three times with deionized water, the samples were air-dried. Cell morphology and staining were assessed using an Axiovert 200 microscope (Carl Zeiss, Germany).

Upon completion of the cultivation, the samples were prepared for examination by scanning electron microscopy (SEM). The samples were washed in 0.1 M phosphate-buffered saline (pH 7.4) and fixed for 12 hours at 5 °C in 2.5 % buffered glutaraldehyde. After fixation, the samples were washed with water and dehydrated at 4°C sequentially in a battery of aqueous ethanol solutions of ascending concentrations (50 %, 75 %, 80 %, 90 %) and in absolute ethanol at the final stage. At each stage, the samples were immersed twice for 5 min in the appropriate ethyl alcohol solution. To remove alcohol, the samples were transferred to hexamethyldisilazane (HMDS) for 30 min, and were air-dried thereafter. The microstructure of the samples was studied using a scanning electron microscope with a Tescan Vega II field emission source (TESCAN, Czech Republic) in secondary electrons (SE type detector) at an accelerating voltage of 20 kV.

The phenotypic expression profile of the cultured cells was assessed by real-time PCR on day 14. The expression of 22 marker genes reflecting osteogenic differentiation processes was studied. The analyzed genes were selected from the database http://www.sabiosciences.com/ for PCR profiling of various biological processes (Table 1).

The gene transcription level was normalized by the average expression levels of the house-keeping genes β-actin and rplp0 (ribosomal protein, large, P0). Gene-specific primers were selected using the Primer Express 3 (Applied Biosystems, USA) (Table 1). The “Isolation of full-length poly (A) mRNA on magnetic particles” kit (Silex, Russia) was used to isolate total matrix RNA from the cells. The resulting mRNA was used to synthesize complementary DNA using the “Synthesis of the first strand of cDNA (oligo (dT) 15)” kit (Eurogen, Russia). cDNA was used as a template for real-time PCR, which was performed on a CFX 96 device (BioRad, USA) using a kit from Eurogen containing the intercalating dye SybrGreen. For this, the reaction mixture was defrosted and thoroughly mixed. The reaction components were mixed in the following sequence (per 25 µl reaction): qPCRmix-HS SYBR — 5 µl, PCR primer 1 — 0.3 µM, PCR primer 2 — 0.3 µM, cDNA template — 1 ng per reaction and sterile water — up to 25 µl. The concentration of primers in the optimization reactions was 0.05 pmol/µl, the concentration of Mg2+ ions was from 1.5 mM, the enzyme concentration was from 0.2 units per 20 µl reaction. The length of the primers was on average 24 nucleotides. Annealing temperature was 60 °C, the length of the amplified fragment was 94–100 nucleotide pairs.

Table 1

Genes which expression was assessed in the study

Abbrivation	Genes name	NCBI Reference Sequence
ALPL	alkaline phosphatase, liver/bone/kidney	NM_000478.4
BGLAP	osteocalcin (bone gamma-carboxyglutamate (gla) protein)	NM_199173.4
BMP1	bone morphogenetic protein 1	NM_006129.4
BMPR1A	bone morphogenetic protein receptor, type IA	NM_004329.2
COL1A1	collagen, type I, alpha 1	NM_000088.3
COL3A1	collagen, type III, alpha 1	NM_000090.3
EGFR	epidermal growth factor receptor	NM_005228.3
FGF-2	fibroblast growth factor 2 (basic)	NM_002006.4
FGFR1	fibroblast growth factor receptor 1	NM_015850.3
IGF1	insulin-like growth factor 1 (somatomedin C)	NM_000618.3
IGFR1	insulin-like growth factor 1 receptor	NM_000875.3
IGF2	insulin-like growth factor 2	NM_000612
RUNX2	runt-related transcription factor 2	NM_004348.3
SMAD2	SMAD family member 2	NM_005901.5
SMAD4	SMAD family member 4	NM_005359.5
SMAD5	SMAD family member 5	NM_005903.6
SPP1	osteopontin-1 (secreted phosphoprotein 1)	NM_000582.2
TGFBR1	transforming growth factor, beta receptor 1	NM_004612.2
TNF	tumor necrosis factor	NM_000594.3
VDR	vitamin D (1,25-dihydroxyvitamin D3) receptor	NM_000376.2
BMP7	bone morphogenetic protein 7	NM_001719.2
TWIST1	twist family bHLH transcription factor 1	NM_000474.3
RPLP0	ribosomal protein, large, P0	NM_001002.3
ACTIN	beta-actin	XM_006715764.1

The reaction was carried out according to the following mode: 1 cycle 95 °C — 5 min; 2–40 cycles 95 °C — 30 sec, 60 °C — 40 sec; 1 cycle (dissociation stage) 95 °C — 15 sec, 60 °C — 1 min, 95 °C — 15 sec. To determine the specificity of the reaction, the amplification products were checked by electrophoresis in 2 % agarose. The specificity of the reaction was also determined from the temperature dissociation curves of the amplicons using the CFX Manager 2.0 program (BioRad, USA). The analysis of data obtained using real-time PCR was performed using the threshold fluorescence method ΔΔC(T), using the web resource for PCR data analysis Qiagen (http://www.qiagen.com); the construction of heat maps of gene expression was performed using the Genesis program (https://genome.tugraz.at/genesisclient/genesisclient_description.shtml).

The obtained expression data were analyzed using the threshold fluorescence method ΔC(T):

$$\Delta C(T)gene = C(T)gene - C(T)\ house\ keeping,$$

where C(T)house keeping is threshold fluorescence house keeping gene.

The difference between gene expression in the experiment and the control was calculated using the method ΔΔC(T):

$$\Delta\Delta C(T)gene = \Delta C(T)gene\ experiment - \Delta C(T)gene\ control.$$

The relative level of gene expression was calculated using the formula:

$$Rel.\ Exper. = 2^{\Delta\Delta C(T)gene}.$$

The online services http://www.qiagen.com/, the Mayday-2.14 program (Center for Bioinformatics Tübingen, Germany) and the Genesis program (Sturn et al., 2002) were used to analyze the data array. The sample without the reverse transcription stage served as a control. Only those results were considered for which changes in the gene expression level were observed at $p < 0.05$.

Statistical processing of the results was performed using the Origin 8.1 program, the standard deviation from the mean was taken as an error; differences according to the Mann – Whitney U-test at $p < 0.05$ were taken as reliable.

RESULTS

Figure 2 and Figure 3 show SEM photographs of carbon scaffolds with and without different types of surface modification in comparison with spongy bone. All the studied samples had a cellular structure consisting of cells communicating with each other, morphologically similar to spongy bone. The size of macropores is in the range from 150 to 200 μm.

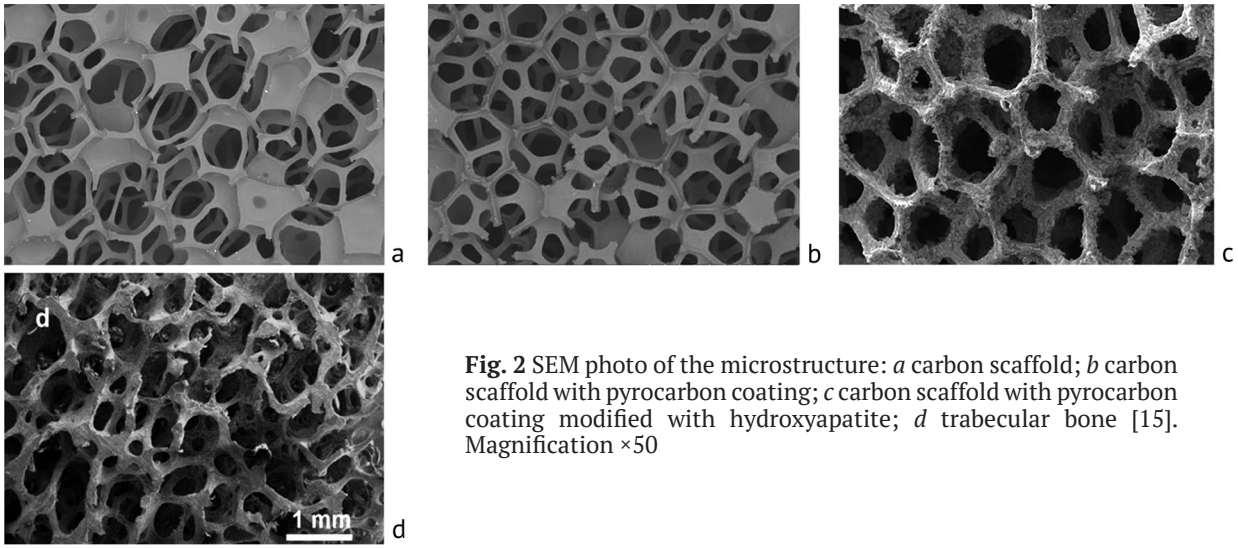

Fig. 2 SEM photo of the microstructure: *a* carbon scaffold; *b* carbon scaffold with pyrocarbon coating; *c* carbon scaffold with pyrocarbon coating modified with hydroxyapatite; *d* trabecular bone [15]. Magnification ×50

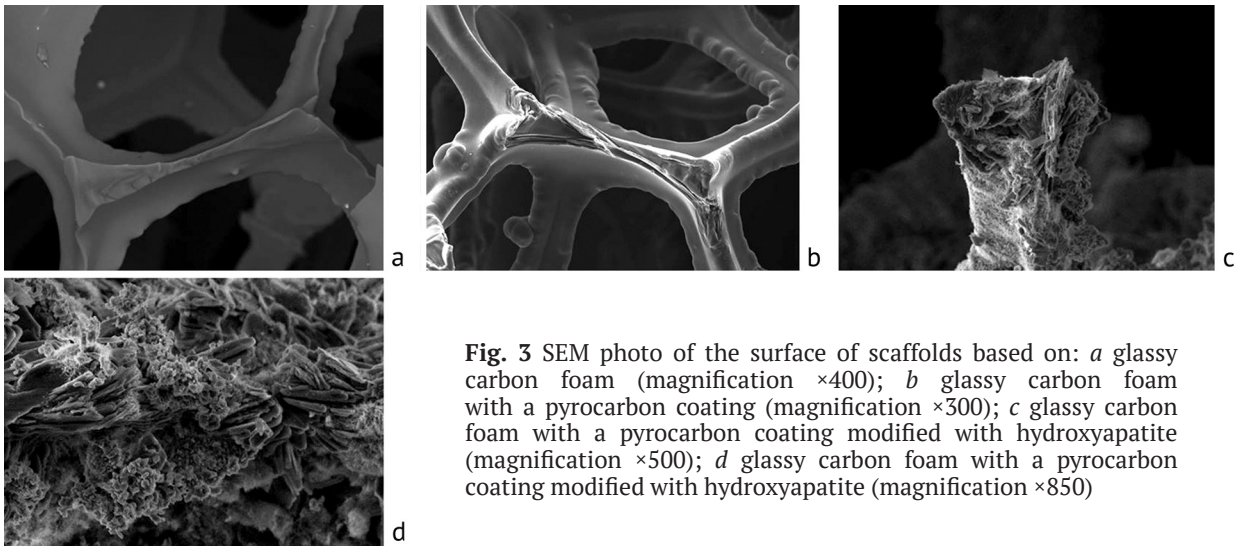

Fig. 3 SEM photo of the surface of scaffolds based on: *a* glassy carbon foam (magnification ×400); *b* glassy carbon foam with a pyrocarbon coating (magnification ×300); *c* glassy carbon foam with a pyrocarbon coating modified with hydroxyapatite (magnification ×500); *d* glassy carbon foam with a pyrocarbon coating modified with hydroxyapatite (magnification ×850)

In terms of their mechanical characteristics, scaffolds used in tissue engineering should be comparable to the characteristics of the bone tissue that should be replaced (Fig. 4).

As can be seen in the presented diagram, the compressive strength of the modified scaffolds was ~ 3 MPa, which is within the range of values for trabecular bone (2 ~ 10 MPa) [16]. The porosity of the studied samples was in the range from 89 to 96 %.

Based on the obtained data, the samples that showed the best results in the physical and mechanical tests, CF-C and CF-C-HAP, were selected for *in vitro* studies.

The study of the metabolic activity of human MSCs showed the absence of toxic effects on the cells of extracts from all the studied materials (Fig. 5).

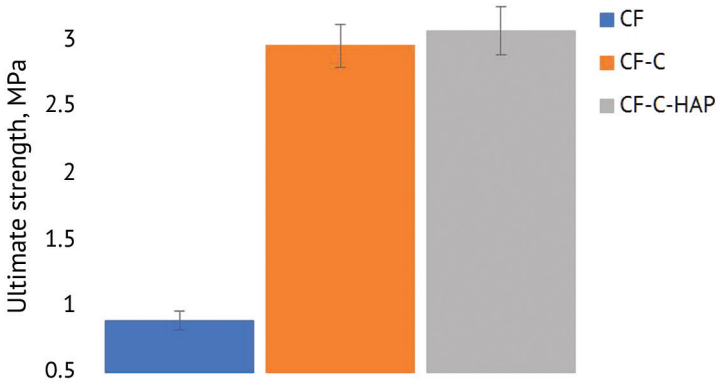

Fig. 4 Compressive strength of carbon scaffolds according to the type of surface modification

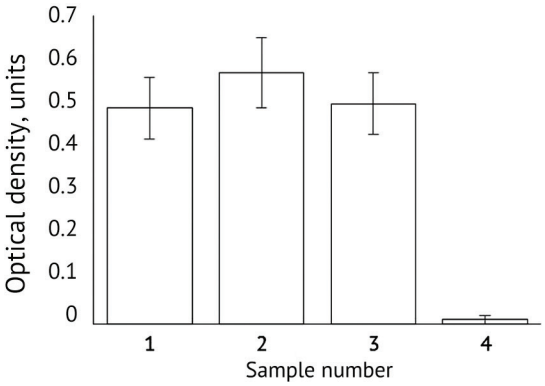

Fig. 5 Metabolic activity of human MSCs based on the results of the MTT test during 48 h incubation with three-day extracts from the studied materials: 1) CF-C; 2) CF-C-HAP; 3) negative control (DMEM/F12 medium); 4) positive control (DMEM/F12 medium + 10 % DMSO)

The results of the study on the viability, adhesive and proliferative activity of human MSCs during cultivation on the surface of carbon scaffolds, carried out using fluorescence microscopy methods, are shown in Figure 6.

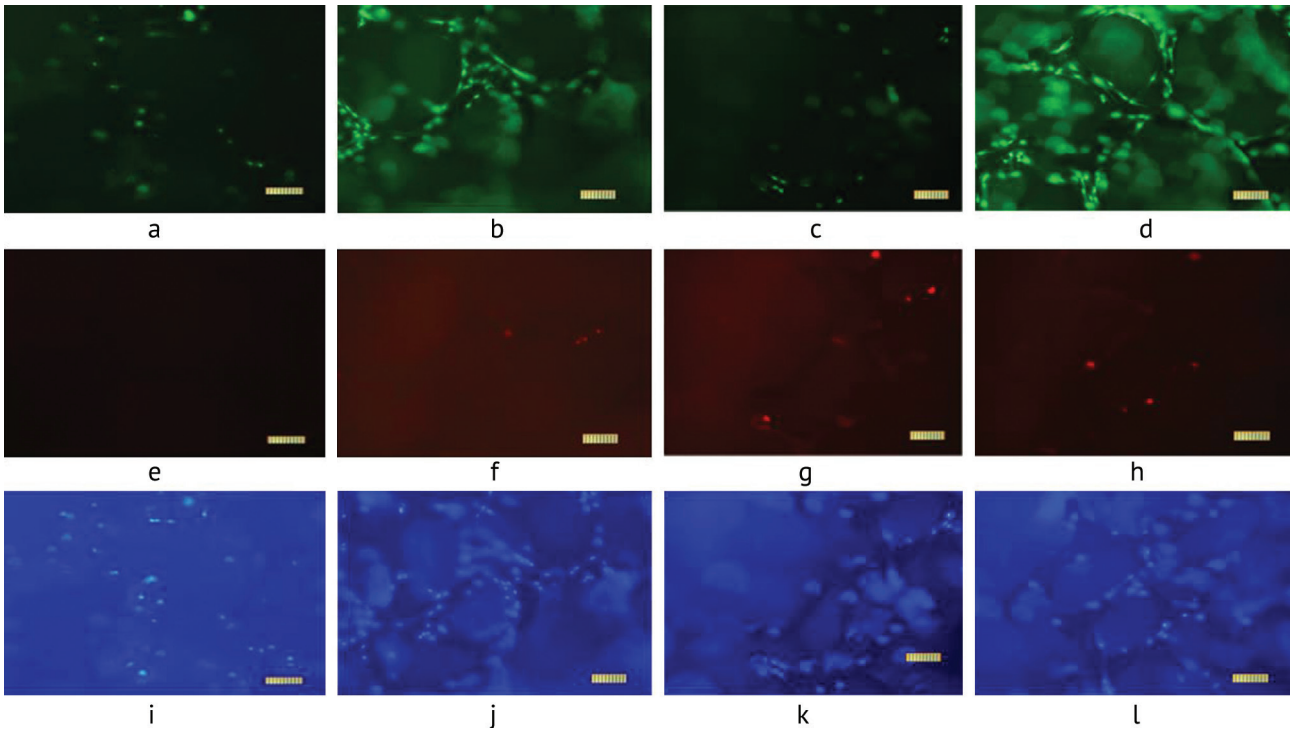

Fig. 6 External human MSCs during cultivation on the surface of CF-C and CF-C-HAP on the seventh (*a, e, i; c, g, k*) and fourteenth (*b, f, j; d, h, l*) days after seeding. Staining SYTO 9 (*a, b, c, d*); PI (*e, f, g, h*); Hoechst 33342 (*i, j, k, l*). Scale bar 100 μm

The differential fluorescent staining method is based on monitoring viable cells depending on the integrity of their membrane. The SYTO 9 dye stains all cells in the culture (green staining), while the disruption of the membrane integrity ensures its permeability for the selective DNA dye propidium iodide (red staining of the nucleus). Hoechst 33342 is a cell permeator (blue staining), staining the DNA of living and dead cells [17].

For control, fluorescent microscopy was performed on cells cultured on a cover glass (Fig. 7).

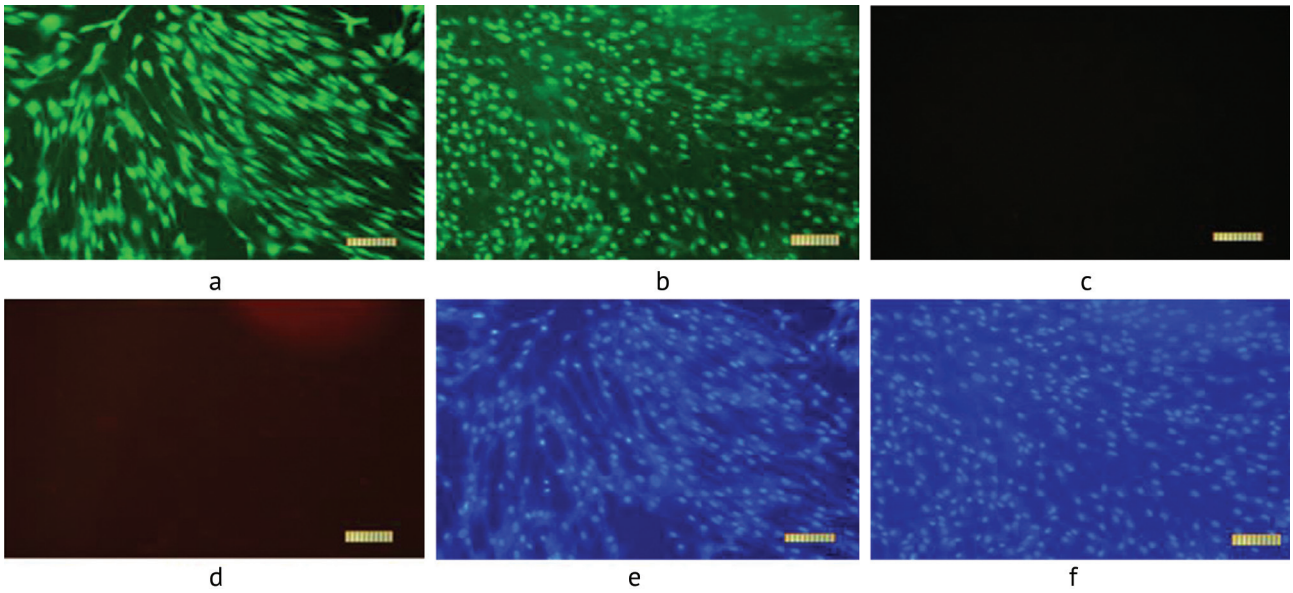

Fig. 7 Appearance of human MSCs during cultivation on the surface of a cover glass (control) on the seventh (*a, c, e*) and fourteenth (*b, d, f*) days after seeding. Staining SYTO 9 (*a, b*); PI (*c, d*); Hoechst 33342 (*e, f*). Scale 100 μm

Also, using SEM, the morphology of the cells was analyzed after culturing for 14 days (Fig. 8).

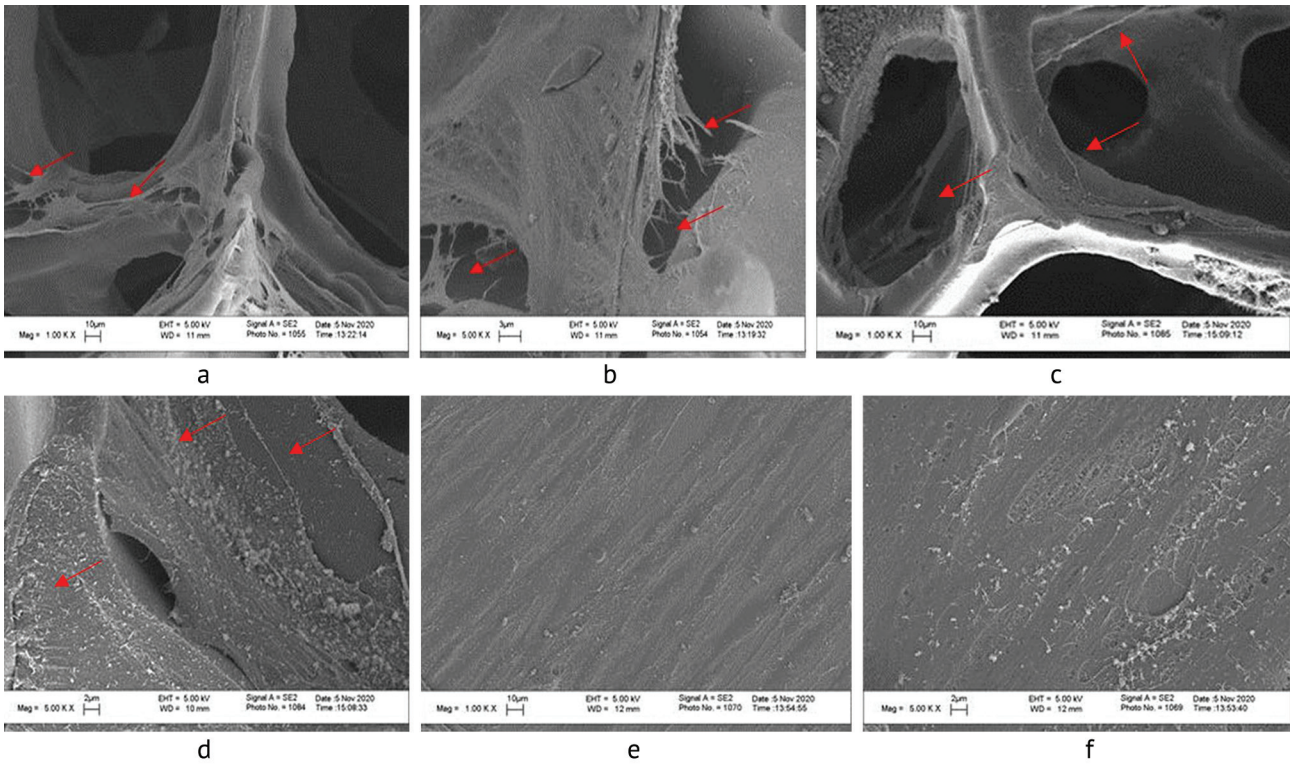

Fig. 8 The appearance of human MSCs cultivated on the surface of: scaffolds based on CF-C (*a* magnification 1000, *b* magnification 5000), CF-C-HAP (*c* magnification ×1000, *d* magnification ×5000) and a cover glass (*e* magnification ×1000, *f* magnification ×5000) on the 14th day after seeding.

Determination of mRNA expression level using real-time PCR Human MSCs cultured on coverslips in DMEM/F12 medium supplemented with 10 % FBS, 100 U/ml penicillin/streptomycin were used as a control.

Comparison of the materials with different surface modifications showed that predominantly similar expression patterns of the studied genes were observed in the cultured cells (Fig. 9, Table 2).

In general, when compared with the control samples, a decrease in the transcriptional activity of all the studied genes was noted, but an increased content of SPP1, VDR and BMP7 gene transcripts was found in B1 samples and in the cells.

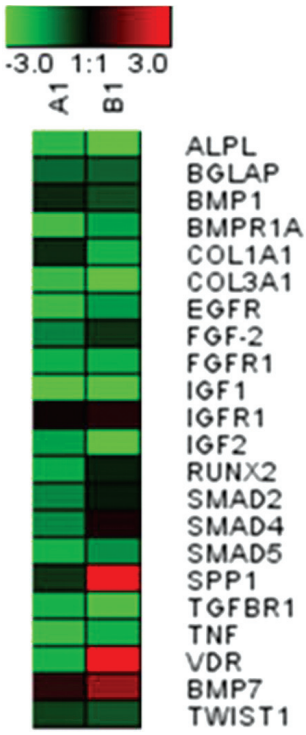

Fig. 9 Gene expression patterns in the cells growing on the samples A1 (CF-C), B1 (CF-C-HAP) in the form of heat maps. In the diagrams: black color - the expression level is comparable to the control; color grading from black to green reflects the degree of inhibition of gene expression, gradations from black to red reflect the level of stimulation relative to the control

Table 2

Gene expression change parameter data from analyzed samples expressed as Log2

Genes	A1	B1
ALPL	−2.28	−3.80
BGLAP	−1.11	−0.76
BMP1	−0.47	−1.21
BMPR1A	−2.57	−1.14
COL1A1	−0.49	−2.50
COL3A1	−2.40	−3.33
EGFR	−2.47	−1.79
FGF-2	−1.40	1.10
FGFR1	−1.95	−1.85
IGF1	−2.90	−1.60
IGFR1	1.14	1.77
IGF2	−1.75	−2.17
RUNX2	−1.85	−0.81
SMAD2	−1.44	−0.59
SMAD4	−1.46	−0.65
SMAD5	−2.05	−1.87
SPP1	−0.58	46.21
TGFBR1	−2.08	−2.23
TNF	−2.49	−1.88
VDR	−2.09	17.51
BMP7	1.44	1.62
TWIST1	−0.73	−0.95

Osteoinductive potential of porous carbon-based matrices The initial stages of osteogenic differentiation of MSCs were analyzed using the Alkaline Phosphatase Kit (Sigma-Aldrich, USA), assessing the histochemical detection of alkaline phosphatase activity in the cells. Alkaline phosphatase, an ectoenzyme secreted by mature osteoblasts, is an early phenotypic marker of MSCs osteogenic differentiation [18–20]. Alkaline phosphatase activity is usually noted *in vitro* on the seventh day after the onset of osteoinduction and is visualized by staining on the 14th day.

To assess the effect of scaffolds on osteogenic differentiation, cells were cultured on the surface of a cover glass, CF-C, CF-C-HAP (Fig. 10).

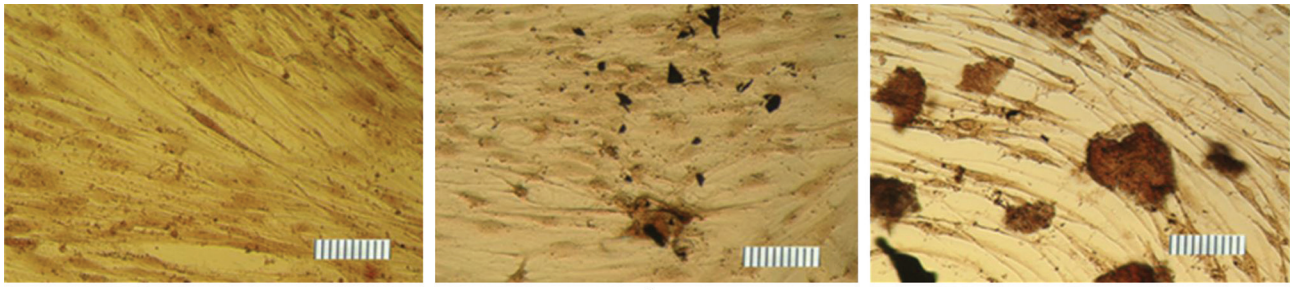

Fig. 10 Alkaline phosphatase activity of human MSCs cultured for 14 days on the surface of material samples: cover glass (*a*), CF-C (*b*); CF-C-HAP (*c*). DMEM/F-12 medium. Scale 100 μm

One of the quantitative methods for determining mineralization during osteogenic differentiation is staining with alizarin red. The appearance of MSCs cultured for 14 days is shown in Fig. 11.

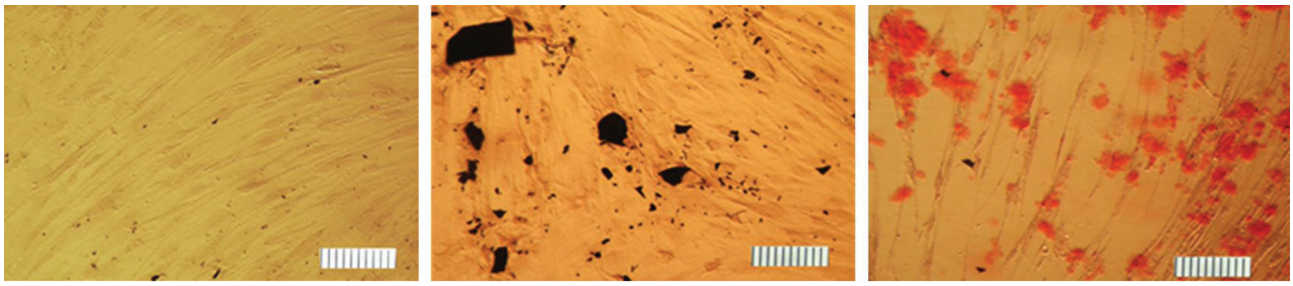

Fig. 11 Appearance of MSCs cultured for 14 days in DMEM/F-12 medium (*a*) and in the presence of CS material samples (*b*); CS-HAP (*c*). Alizarin red staining. Scale bar 100 μm

DISCUSSION

One of the main tasks of tissue engineering is the development of a scaffold that imitates the three-dimensional architecture for osteogenic progenitor cells inside the scaffold that are able to interact with the corresponding chemical and physical stimuli of the natural bone [21]. Despite a significant research conducted in this area, the requirements for the design of scaffolds for tissue engineering have not been fully formulated. However, a number of key structural characteristics are identified that determine the possibility of intercellular interactions inside the scaffold. It is known that pore size, the degree of canal interconnectivity, as well as overall porosity play a decisive role in regulating the morphology and behavior of various cell types [1, 22–25]. Porosity and pore size make a significant contribution to the ability of the scaffold to maintain cell adhesion, which, in turn, has an impact on the cell population density in the scaffold volume, as well as on their distribution and migration [24, 26]. The pore sizes required by different cell types vary significantly, but on average, a pore size range of 100–500 μm is acceptable for efficient cell growth, migration, nutrient penetration, and waste removal. Increasing the pore size of the scaffold reduces the surface area, limits cell adhesion, and prevents the formation of protein-cell bridges. Moreover, the mechanical properties of the scaffold are impaired by increased empty spaces, which is another critical parameter in the design [17, 22]. For scaffolds intended for bone tissue regeneration, a pore size in the range of 150–400 μm is optimal for stimulating osteogenesis and vascularization deep into the tissue-engineered construct [22, 27].

In this study, we propose a technically simple and inexpensive method for obtaining scaffolds that imitate the structure of human trabecular bone tissue. Glassy carbon foam was chosen as the base for the composite scaffold. Glassy carbon foam based on a polyurethane template is a three-dimensional structure with a pore size of 150–200 μm, open porosity, mainly consisting of carbon. The pores in this range facilitate the infiltration of cells involved in proliferation, migration, and vascularization *in vivo* [27].

Due to the cellular structure and bioinertness, glassy carbon foams are suitable for use as scaffolds in tissue engineering [28, 29]. The most important characteristics of the material for use as scaffolds are porosity, strength, lack of toxicity, along with osteoinductivity and osteoconductivity [22, 30]. The scaffold material should have the strength comparable to the strength of the replaced tissue. Since glassy carbon foams are brittle materials, their strength characteristics are assessed by the compressive strength [28]. The compressive strength and elastic modulus of glassy carbon foams depend primarily on such parameters as volumetric density and porosity. It is extremely important to maintain high open porosity of scaffolds, since this favors cell adhesion and proliferation [27, 31]. One of the ways to improve strength characteristics is surface modification by applying various coatings. Pyrocarbon deposition allowed increasing the compressive strength to ~3 MPa, while

maintaining the overall porosity at 93 %. The high porosity of the scaffold due to the large surface area ensures greater interaction with the extracellular matrix [32], which in turn promotes bone tissue ingrowth and vascularization [32]. Moreover, constant contact of the scaffold with the extracellular matrix over time leads to pore occlusion. Therefore, high porosity of the scaffold ensures sufficient permeability for the transport of nutrients and biomolecules [32].

To improve the osteoinductive properties of the scaffold, the surface was additionally modified with hydroxyapatite [27, 33]. SEM studies showed that the resulting coating is formed on both the external and internal surfaces of the scaffold, is homogeneous, and consists predominantly of lamellar hydroxyapatite crystals. The application of the hydroxyapatite coating resulted in a slight increase in strength characteristics, which is consistent with the results obtained in the work of Rahman et al [27].

The study of the metabolic activity of human MSCs showed the absence of toxic effects on the cells of extracts from all the studied materials. At the same time, a slight increase in the optical density of the solution to which the extract from CF-C-HAP was added was noted (Fig. 5). It may indicate the presence of water-soluble factors stimulating cell activity. However, statistical analysis of the results of the study of the metabolic activity of DPSC cells that was carried out using the nonparametric Mann-Whitney U criterion did not show significant differences with the control when the cells were exposed to extracts from all materials. Thus, it can be concluded that all the materials studied by us did not exhibit cytotoxicity and that there were no water-soluble components that affected the viability of human MSCs.

Studies of MSCs viability, adhesion and proliferative activity showed that at all experiment observation periods for CF-C and CF-C-HAP, adherent cells were detected, and the dynamics of their density increased during the observation periods. On the 14th day after incubation, a dense arrangement of cells was observed both on the surface and inside the three-dimensional scaffolds (Fig. 6).

SEM analysis of cell attachment and morphology showed that the cells actively proliferated on the surface of scaffolds modified with both pyrocarbon and hydroxyapatite. Modification of the surface of carbon scaffolds leads to the appearance of roughness (Fig. 2 b, c), which, in turn, is one of the factors stimulating osteogenesis [34].

The cells formed a dense monolayer growing through pores within the three-dimensional carbon scaffold. The cells were elongated with a flat surface and have extensive filopodia (Fig. 8 a, b), indicating strong cell adhesion and growth.

Determination of the mRNA expression level using the real-time PCR method showed (Table 2) that the cells cultured on CS-C-HAP showed gene expression after 14 days. VDR encodes the vitamin D3 receptor, which regulates the activity of mineral metabolism genes and controls calcium and phosphorus homeostasis [35, 36]. BMP7 is a stimulator of osteoblast differentiation, which is necessary for the differentiation of preosteoblasts into mature osteoblasts [37]. IGFR1 is an important regulator of bone tissue homeostasis, which probably stimulates the replication and differentiation of osteoblasts [38, 39], and also increases the expression of type I collagen in osteoblasts and reduces the transcription of matrix metalloproteinase (MMP)-13 [40], which destroys collagen fibers and bones [41]. SPP1 is a glycoprotein involved in osteogenesis [42–44], enhances differentiation and proliferation of osteoblasts [42, 44, 45], and modulates both bone formation and resorption due to the attachment of osteoclasts to the mineralized bone matrix [45]. Based on the data on the increase in the expression of genes associated with osteogenesis, it can be concluded that the developed materials have osteogenic potential.

Osteogenesis is the process of new bone formation that involves calcification of the pre-bone matrix and differentiation of osteoblasts, the precursors of bone tissue, into mature osteocytes. Matrix mineralization or calcification in osteoinduced MSCs can be detected by ALP activity and alizarin red

staining. After 14 days of induction, a small number of ALP-positive cells were observed on the CF-C surface. Cells cultured on the CF-C-HAP surface (Fig. 10 c) showed higher ALP activity compared to Figure 10 a and 10 b. Alizarin red staining of the cultured cells showed that spontaneous osteogenic differentiation was absent in the control (Fig. 11 a). Staining of the MSC culture in the presence of CF-C gave a negative result similar to the control, indicating the absence of mineralization and differentiation in the osteogenic direction (Fig. 11 b). In the presence of CF-C-HAP (Fig. 11 c), cell clusters shaped as osteoblast nodules and deposits of extracellular matrix were observed, revealed histochemically by staining with alizarin red as calcifications, indicating its ability to induce MSC differentiation in the osteogenic direction and produce calcium-containing matrix.

The results of our studies on phosphatase activity and alizarin red staining showed that the CF-C-HAP scaffold stimulates osteoblast differentiation *in vitro* in the osteogenic direction, along with intracellular mineralization processes in osteoblasts.

CONCLUSION

Carbon scaffolds based on glassy carbon foam with a hydroxyapatite-modified surface have high porosity, developed surface, and reproduce the architecture of trabecular bone tissue. Application of a pyrolytic carbon-based coating helps to increase the strength characteristics and reduces the hydrophobicity of the carbon scaffold. Modification with hydroxyapatite significantly increases the roughness of the material, which has a positive effect on adhesion and cell attachment. All carbon scaffolds studied in the work showed no cytotoxicity.

It was found that scaffolds modified with hydroxyapatite possess osteoinductivity, are capable of inducing MSC differentiation in the osteogenic direction, producing a calcium-containing matrix and increasing the expression of genes associated with osteogenesis.

The material thus developed is promising for use in tissue engineering.

Conflict of interests *The authors declare no conflict of interest.*

Funding *The work was sponsored by the State Corporation Rosatom.*

Ethical approval *Not required*

Informed consent *Not applicable*

REFERENCES

1. Sadovoy MA, Larionov PM, Samokhin AG, Rozhnova OM. Cellular matrices (scaffolds) for bone regeneration: state of the art. *Russian Journal of Spine Surgery*. 2014;2:79-86. (In Russ.) doi: 10.14531/ss2014.2.79-86.
2. Phadke A, Hwang Y, Kim SH, et al. Effect of scaffold microarchitecture on osteogenic differentiation of human mesenchymal stem cells. Eur Cell Mater. 2013;25:114-129. doi: 10.22203/ecm.v025a08.
3. Taylor B, Indano S, Yankannah Y, et al. Decellularized Cortical Bone Scaffold Promotes Organized Neovascularization In Vivo. Tissue Eng Part A. 2019;25(13-14):964-977. doi: 10.1089/ten.TEA.2018.0225.
4. Sohn HS, Oh JK. Review of bone graft and bone substitutes with an emphasis on fracture surgeries. Biomater Res. 2019;23:9. doi: 10.1186/s40824-019-0157-y.
5. Chiarello E, Cadossi M, Tedesco G, et al. Autograft, allograft and bone substitutes in reconstructive orthopedic surgery. Aging Clin Exp Res. 2013;25 Suppl 1:S101-S103. doi: 10.1007/s40520-013-0088-8.
6. Hatzenbuehler J, Pulling TJ. Diagnosis and management of osteomyelitis. Am Fam Physician. 2011 Nov 1;84(9):1027-1033.
7. Wang W, Zhang Y, Liu W. Bioinspired fabrication of high strength hydrogels from non-covalent interactions. Prog Polym Sci. 2017;71:1-25. doi: 10.1016/j.progpolymsci.2017.04.001.
8. Zamborsky R, Svec A, Bohac M, et al. Infection in bone allograft transplants. Exp Clin Transplant. 2016;14(5):484-490. doi: 10.6002/ect.2016.0076.
9. Oakley MJ, Smith WR, Morgan SJ, ey al. Repetitive posterior iliac crest autograft harvest resulting in an unstable pelvic fracture and infected non-union: case report and review of the literature. Patient Saf Surg. 2007;1(1):6. doi: 10.1186/1754-9493-1-6.
10. Gao Y, Ma Q. Bacterial infection microenvironment-responsive porous microspheres by microfluidics for promoting anti-infective therapy. Smart Med. 2022;1(1):e20220012. doi: 10.1002/SMMD.20220012.
11. Zhu Y, Kong B, Liu R, Zhao Y. Developing biomedical engineering technologies for reproductive medicine. Smart Med. 2022;1(1):e20220006. doi: 10.1002/SMMD.20220006.
12. Dixon DT, Gomillion CT. Conductive Scaffolds for Bone Tissue Engineering: Current State and Future Outlook. J Funct Biomater. 2021;13(1):1. doi: 10.3390/jfb13010001.
13. Perez JR, Kouroupis D, Li DJ, et al. Tissue Engineering and Cell-Based Therapies for Fractures and Bone Defects. Front Bioeng Biotechnol. 2018;6:105. doi: 10.3389/fbioe.2018.00105.
14. Liu H, Xia L, Dai Y, et al. Fabrication and characterization of novel hydroxyapatite/porous carbon composite scaffolds. Materials Letters. 2012;66(1):36-38. doi: 10.1016/j.matlet.2011.08.053.
15. Guillén T, Ohrndorf A, Tozzi G, et al. Compressive fatigue behavior of bovine cancellous bone and bone analogous materials under multi-step loading conditions. Advanced Engineering Materials. 2012;14(5):B199-B207. doi: 10.1002/adem.201180060.

16. Ramaswamy G, Bidez MW, Misch CE. Bone response to mechanical loads. In: Misch CE. Dental Implant Prosthetics (Second Edition). Mosby; 2015:107-125. doi: 10.1016/B978-0-323-07845-0.00006-3.
17. Popov AL, Tatarnikova OG, Shekunova TO, et al. The influence of nanocrystalline gadolinium-doped ceria (Ce1–xGdxO2–y) on the functional status and viability of NCTC clone L929. *Vestn Tomskogo Gos Univ. Khimiya*. 2017;(8):68-87. doi: 10.17223/24135542/8/6.
18. Wutticharoenmongkol P, Pavasant P, Supaphol P. Osteoblastic phenotype expression of MC3T3-E1 cultured on electrospun polycaprolactone fiber mats filled with hydroxyapatite nanoparticles. Biomacromolecules. 2007;8(8):2602-2610. doi: 10.1021/bm700451p.
19. Tsukamoto Y, Fukutani S, Mori M. Hydroxyapatite-induced alkaline-phosphatase activity of human pulp fibroblasts. J Mater Sci: Mater Med. 1992;3:180-183. doi: 10.1007/bf00713446.
20. Lao L, Wang Y, Zhu Y, et al. Poly(lactide-co-glycolide)/hydroxyapatite nanofibrous scaffolds fabricated by electrospinning for bone tissue engineering. J Mater Sci Mater Med. 2011;22(8):1873-1884. doi: 10.1007/s10856-011-4374-8.
21. Chung S, King MW. Design concepts and strategies for tissue engineering scaffolds. Biotechnol Appl Biochem. 2011;58(6):423-438. doi: 10.1002/bab.60.
22. Saberi A, Kouhjani M, Mohammadi M, Hosta-Rigau L. Novel scaffold platforms for simultaneous induction osteogenesis and angiogenesis in bone tissue engineering: a cutting-edge approach. J Nanobiotechnology. 2023;21(1):351. doi: 10.1186/s12951-023-02115-7.
23. He X, Zhao Q, Zhang N, et al. Impact of a staggered scaffold structure on the mechanical properties and cell response in bone tissue engineering. J Appl Biomater Funct Mater. 2023;21:22808000231181326. doi: 10.1177/22808000231181326.
24. Abbasi N, Hamlet S, Love RM, Nguyen NT. Porous Scaffolds for Bone Regeneration. J Sci: Adv Mater Dev. 2020;5(1):1-9. doi: 10.1016/j.jsamd.2020.01.007.
25. Aghali A. Craniofacial Bone Tissue Engineering: Current Approaches and Potential Therapy. Cells. 2021;10(11):2993. doi: 10.3390/cells10112993.
26. Persson M, Lehenkari PP, Berglin L, et al. Osteogenic differentiation of human mesenchymal stem cells in a 3D woven scaffold. Sci Rep. 2018;8(1):10457. doi: 10.1038/s41598-018-28699-x.
27. Rahman SF, Ghiffary MM, Tampubuluon JY, et al. Effect of graphite, graphene oxide, and multi-walled carbon nanotubes on the physicochemical characteristics and biocompatibility of chitosan/hyaluronic acid/hydroxyapatite scaffolds for tissue engineering applications. J Sci: Adv Mater Dev. 2024;9(2):100719. doi: 10.1016/j.jsamd.2024.100719.
28. Bagal R, Bahir M, Lenka N, Patro TU. Polymer derived porous carbon foam and its application in bone tissue engineering: a review. Int J Polymer Mater Polymer Biomat. 2022;72(12):909-924. doi: 10.1080/00914037.2022.2066669.
29. Islam M, Sadaf A, Gomez MR, et al. Carbon fiber/microlattice 3D hybrid architecture as multi-scale scaffold for tissue engineering. Mater Sci Eng C Mater Biol Appl. 2021;126:112140. doi: 10.1016/j.msec.2021.112140.
30. Dong J, Ding H, Wang Q, Wang L. A 3D-Printed Scaffold for Repairing Bone Defects. Polymers (Basel). 2024;16(5):706. doi: 10.3390/polym16050706.
31. Lee DJ, Kwon J, Kim YI, et al. Effect of pore size in bone regeneration using polydopamine-laced hydroxyapatite collagen calcium silicate scaffolds fabricated by 3D mould printing technology. Orthod Craniofac Res. 2019;22 Suppl 1(Suppl 1):127-133. doi: 10.1111/ocr.12261.
32. Koushik TM, Miller CM, Antunes E. Bone tissue engineering scaffolds: function of multi-material hierarchically structured scaffolds. Adv Healthc Mater. 2023;12(9):e2202766. doi: 10.1002/adhm.202202766.
33. Cao J, Lian R, Jiang X, Rogachev AV. In vitro degradation assessment of calcium fluoride-doped hydroxyapatite coating prepared by pulsed laser deposition. Surface and Coatings Technology. 2021;416:127177. doi: 10.1016/j.surfcoat.2021.127177.
34. Zhang Y, Chen SE, Shao J, van den Beucken JJJP. Combinatorial Surface Roughness Effects on Osteoclastogenesis and Osteogenesis. ACS Appl Mater Interfaces. 2018;10(43):36652-36663. doi: 10.1021/acsami.8b10992.
35. Meyer MB, Goetsch PD, Pike JW. Genome-wide analysis of the VDR/RXR cistrome in osteoblast cells provides new mechanistic insight into the actions of the vitamin D hormone. J Steroid Biochem Mol Biol. 2010;121(1-2):136-141. doi: 10.1016/j.jsbmb.2010.02.011.
36. Li Y, Zhao P, Jiang B, et al. Modulation of the vitamin D/vitamin D receptor system in osteoporosis pathogenesis: insights and therapeutic approaches. J Orthop Surg Res. 2023; 18(1):860. doi: 10.1186/s13018-023-04320-4.
37. Ott SM, Elder G. Osteoporosis associated with chronic kidney disease. In: Marcus R, Feldman D, Dempster DW, et al. (eds). Osteoporosis. 4th ed. Elsevier Pub.; 2013:1387-1424. doi: 10.1016/B978-0-12-415853-5.00058-3.
38. Yakar S, Rosen CJ. From mouse to man: redefining the role of insulin-like growth factor-I in the acquisition of bone mass. Exp Biol Med (Maywood). 2003;228(3):245-252. doi: 10.1177/153537020322800302.
39. Fang J, Zhang X, Chen X, et al. The role of insulin-like growth factor-1 in bone remodeling: A review. Int J Biol Macromol. 2023;238:124125. doi: 10.1016/j.ijbiomac.2023.124125.
40. Canalis E, Rydziel S, Delany AM, et al. Insulin-like growth factors inhibit interstitial collagenase synthesis in bone cell cultures. Endocrinology. 1995;136:1348-1354. doi: 10.1210/endo.136.4.7895645.
41. Brennan-Speranza TC, Rizzoli R, Kream BE, et al. Selective osteoblast overexpression of IGF-I in mice prevents low protein-induced deterioration of bone strength and material level properties. Bone. 2011;49(5):1073-1079. doi: 10.1016/j.bone.2011.07.039.
42. Denhardt DT, Noda M. Osteopontin expression and function: Role in bone remodeling. J Cell Biochem. 1998;72 Suppl 30-31(S30-31):92-102. doi: 10.1002/(SICI)1097-4644(1998)72:30/31+<92::AID-JCB13>3.0.CO;2-A.
43. Choi ST, Kim JH, Kang EJ, et al Osteopontin might be involved in bone remodelling rather than in inflammation in ankylosing spondylitis. Rheumatology (Oxford). 2008;47(12):1775-1779. doi: 10.1093/rheumatology/ken385.
44. Martín-Márquez BT, Sandoval-García F, Corona-Meraz FI, et al. Osteopontin: A Bone-Derived Protein Involved in Rheumatoid Arthritis and Osteoarthritis Immunopathology. Biomolecules. 2023;13(3):502. doi: 10.3390/biom13030502.
45. Singh A, Gill G, Kaur H, et al. Role of osteopontin in bone remodeling and orthodontic tooth movement: a review. Prog Orthod. 2018;19(1):18. doi: 10.1186/s40510-018-0216-2.

The article was submitted 18.07.2024; approved after reviewing 26.09.2024; accepted for publication 10.12.2024.

Information about the authors:

Elena I. Timoshchuk — PhD in Engineering, Head of Structural Materials Department, EITimoschuk@rosatom.ru, https://orcid.org/0009-0003-4162-1196;

Darya V. Ponomareva — Deputy Head of Department — Head of Structural Graphite Department, DVPonomareva@rosatom.ru, https://orcid.org/0009-0009-4886-1436;

Artur R. Gareev — PhD in Engineering, Deputy Director for Science and Innovation, ARGareev@rosatom.ru, https://orcid.org/0000-0001-5934-8456.